SOME EXPERIMENTAL OBSERVATIONS OF THE ATTENUATION OF ALFVEN WAVES IN A LABORATORY PLASMA

By I. G. Brown*

[*Manuscript received June 2, 1965*]

Summary

An experiment is described in which the velocity and attenuation of torsional, azimuthally symmetric, hydromagnetic waves are measured in a hydrogenous plasma, from low frequencies where ion–neutral collisions are unimportant to the wave damping, to frequencies where such collisions profoundly affect the damping. A theory including both ion–electron and ion–neutral collisions is outlined, and the attenuation results are compared with the theoretical values. An estimate is made, from the frequency dependence of the attenuation, of the hydrogen ion–atom collision cross section for momentum transfer.

I. Introduction

A conducting fluid contained in a magnetic field is capable of supporting a large number of different types of wave motions. The type that results from the interaction of electromagnetic and hydrodynamic forces is known, at frequencies below ion cyclotron frequency, as a hydromagnetic wave. The case of propagation parallel to the static magnetic field was first considered theoretically by Alfvén (1942) in an attempt to explain the zone velocity and long period of sunspots. The theory was carried further by Åström (1950*a*, 1950*b*) and Herlofson (1950), and since then by many authors.

The first laboratory demonstrations of Alfven waves, as these waves are also called, were carried out by Lundquist (1949) in mercury, and by Lehnert (1954) in sodium. The wave attenuation in these liquid metals is quite high; a much lower attentuation is possible when the wave is propagated in a plasma. Bostik and Levine (1952) observed standing hydromagnetic waves in a toroidal helium plasma.

More recently, Alfven wave experiments have been conducted at Berkeley, California, at Tohoku, Japan, and at Culham, England. At Berkeley, Allen *et al.* (1959) launched waves in a cylindrical deuterium plasma and measured the velocity and attenuation; the velocity results were consistent with theory, but the attenuation results were not explained at that time. De Silva (1961) carried the experiment further, and for waves of frequency much less than the ion–neutral collision frequency was able to explain the attenuation in terms of ion–electron collisions. Spillman (1963) extended the measurements to frequencies comparable with the ion–neutral collision frequency; his results, however, were in only qualitative agreement with the theory that took these collisions into account. Nagao and Sato (1960, 1961), at Tohoku, using an air plasma, have also demonstrated the propagation of these waves. At Culham, Jephcott and Stocker (1962) investigated their propagation in helium and argon plasmas for frequencies approaching the ion cyclotron frequency.

* Wills Plasma Physics Department, School of Physics, University of Sydney.

They obtained good agreement for both velocity and attenuation with the theory of Woods (1962) if a loss of particles from the plasma is assumed.

In the experiment described here, the wave velocity and attenuation in a hydrogen plasma are measured, from low frequencies to frequencies where ion–neutral collisions significantly affect the wave attenuation. The attenuation results are compared with a theory that includes both ion–electron and ion–neutral collisions. Further, the measured frequency-dependence of the attenuation allows an estimate to be made of the ion–neutral collision cross section for momentum transfer.

II. Theory

The attenuation or damping length L is defined as that distance in the direction of propagation in which the amplitude of the wave field decreases by a factor e. If the wave is propagating in the z (axial) direction, is of angular frequency ω, and has propagation constant p, then all wave variables vary as $\exp i(pz-\omega t)$; for propagation in a cylindrical geometry, azimuthal symmetry is assumed. The real and imaginary parts of p are respectively the wave number κ and the attenuation constant ϵ, that is, $p = \kappa+i\epsilon$; κ and ϵ are related to the wavelength λ and the attenuation length L by $\kappa = 2\pi/\lambda$ and $\epsilon = 1/L$. If one obtains the dispersion relation for hydromagnetic waves in a cylindrical plasma, then the wave attenuation can be predicted in terms of the various plasma parameters.

The theoretical model assumed is as follows. A partially ionized hydrogenous plasma of finite conductivity is contained in a cylindrical, perfectly conducting waveguide, infinite in one direction. The plasma is uniform throughout its volume, except for perhaps a thin layer of vacuum (cold gas) between it and the wall. A steady axial magnetic field exists throughout the entire region, and the wave magnetic field is a small perturbation on this. Electron–neutral collisions are neglected and only azimuthally symmetric ($m = 0$) waves are considered.

(a) *Dispersion Relation*

The dispersion relation is derived in the Appendix. It is obtained by eliminating in turn all variables but one (here, the wave magnetic field $\mathbf{b}$) from the equations of motion for ions, electrons, and neutral atoms, Maxwell's equations, and various conservation laws and definitions. The condition for a non-trivial solution to the resulting equation in $\mathbf{b}$, i.e. that the determinant of coefficients vanishes, gives the dispersion relation.

The dispersion relation is

$$ap^4+bp^2+c = 0,$$

where a, b, c are algebraic functions of the plasma parameters and are defined in the Appendix. This equation is quadratic in p^2 and so has two distinct roots, corresponding to two wave types. These are known variously as:

(i) Torsional, shear, T-type, or slow wave. This wave is left-hand polarized, that is, its electric field vector rotates about the static magnetic field in the same sense as the ions. It hence has a resonance at the ion cyclotron frequency, and is heavily damped for higher frequencies. For frequencies much less than the ion cyclotron frequency this wave is the ordinary Alfven wave.

(ii) Compressional, TLA-type, or fast wave. This wave has, in a cylindrical geometry, a low frequency cut-off for angular frequencies less than $\omega_C = \nu V_A$, where ν is the radial wave number and V_A the Alfven speed. Its polarization is right-handed and hence it has a resonance at the electron cyclotron frequency. For frequencies approaching this frequency it is known as the Whistler wave.

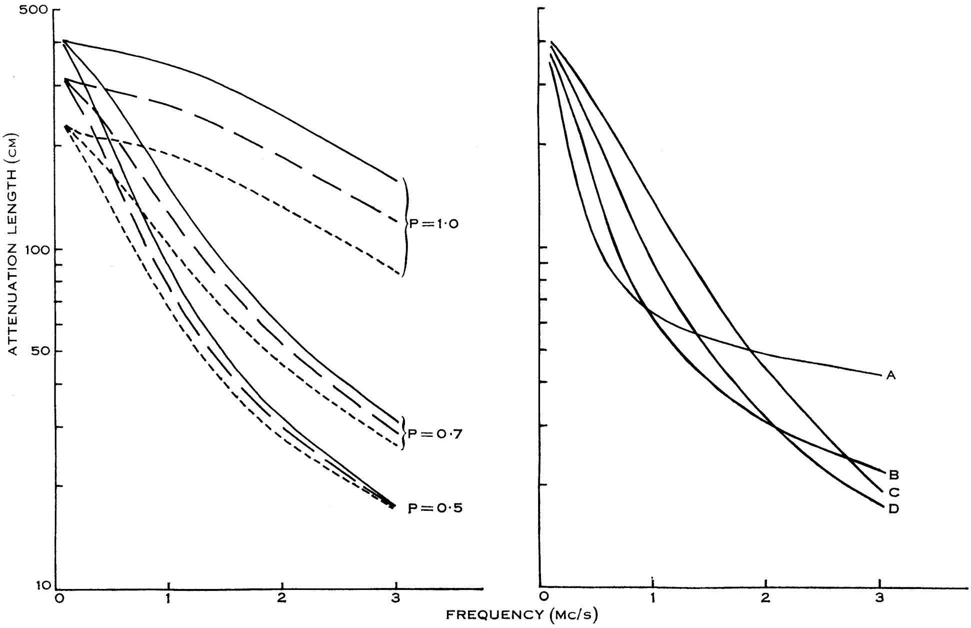

Fig. 1 Fig. 2

Fig. 1.—Theoretical attenuation length as a function of frequency for variation of fractional ionization and temperature. Fractional ionizations are 1·0, 0·7, 0·5 and temperatures are 1·2 (——), 1·0 (— —), 0·8 (– – –) $\times 10^4$ °K. Other parameters are: axial magnetic field 12·8 kG, total particle density $2 \cdot 1 \times 10^{15}$ cm^{-3}, radial wave number 36·5 m^{-1}, cross section $1 \cdot 0 \times 10^{-14}$ cm^2.

Fig. 2.—Theoretical attenuation length as a function of frequency for variation of cross section. Cross sections are: A 2·0, B 5·0, C 20·0, D $10 \cdot 0 \times 10^{-15}$ cm^2. Other parameters are: axial magnetic field 12·8 kG, total particle density $2 \cdot 1 \times 10^{15}$ cm^{-3}, radial wave number 36·5 m^{-1}, fractional ionization 0·5, temperature $1 \cdot 2 \times 10^4$ °K.

The torsional hydromagnetic wave is the one studied in the present experiment. For the plasma parameters employed here the fast wave is cut off (i.e. is highly attenuated) for frequencies less than 3·5 Mc/s, which is greater than the maximum frequency used.

The dispersion relation for the torsional mode has been numerically evaluated using the English–Electric KDF9 computer. In particular, the damping length has been plotted as a function of frequency for many different sets of plasma parameters. Some of these curves, demonstrating the general trends, are shown in Figures 1 and 2. It should be noted that the dispersion relation used here differs from that of De Silva (1961) and Spillman (1963) in that the parallel and transverse resistivities are not approximated to equality. This assumption of equality gives rise to quite different attenuations, especially at high percentage ionizations when there is little neutral damping; for a fully ionized plasma at a temperature of 1 eV the error is nearly a factor of two at a few megacycles per second.

(b) *Wave Radial Mode Number*

The attenuation length (and to a considerably smaller extent the phase velocity) is dependent on the radial mode number; higher-order modes are damped out more rapidly than are lower modes. For comparison with theory then, it is necessary to know with which mode we are dealing, or, if there are more than one, what percentages of the various modes are present. Three points of relevance here are: (i) the relative amplitudes at the launching electrode, (ii) the relative attenuations, and (iii) the relative amplitudes of the various modes at the radius of the probe (owing to different radial variations of the azimuthal component of the wave magnetic field, b_θ).

Table 1

Relative amplitudes of first five radial modes of the torsional hydromagnetic wave

Radial Mode Number	Max. Amplitude at $z = 0$	Attenuation Length at 1 Mc/s (cm)	Max. Amplitude at $z = 50$ cm	Amplitude at Radius of Probe (for $z = 50$ cm)
1	$+1$	75	$+1$	$+1$
2	$-0\cdot37$	52	$-0\cdot28$	$-0\cdot096$
3	$-0\cdot15$	35	$-0\cdot07$	$+0\cdot037$
4	$-0\cdot46$	26	$-0\cdot13$	$+0\cdot047$
5	$+0\cdot34$	19	$+0\cdot048$	$+0\cdot018$

(i) The relative amplitudes at the launching electrode are determined by the radii of the inner and outer electrodes, and by the boundary condition imposed on b_θ (or its equivalent, E_r) at the quartz plate at the launching end. These have been calculated and are given in the second column of Table 1.

(ii) The radial wave number ν_n appropriate to the nth radial mode is obtained as the solution to $\mathrm{J}_1(\nu_n R) = 0$, where J_1 is the Bessel function of the first kind and order, and R is the vessel radius. This results from the boundary condition imposed on b_θ by the conducting walls. If there is a layer of cold gas between plasma and wall, this simple expression is replaced by a more complicated one; but it happens that for a thin vacuum layer the change in ν_n is small, smaller than would be obtained from a direct reduction in the value of R to the plasma radius. Hence, with the vessel radius for R, and using the simple expression to find the appropriate ν_n, the attenuation lengths for the present plasma have been calculated from the dispersion relation and are shown in the third column of Table 1 for a typical frequency. The effect of different attenuation lengths on the relative amplitudes, at a distance of 50 cm, is shown in the fourth column of the table.

(iii) The magnetic probe is inserted into the plasma at a radial distance for which the lowest-order mode of b_θ has a maximum; higher modes have their maxima elsewhere. This further reduced the amplitudes of the monitored wave fields of higher modes, as is shown by the values given in the final column of Table 1. It is clear from this table that for the experimental arrangement used the wave field monitored is, to a good approximation, only the lowest mode.

III. Experimental Method

(a) Apparatus

The experiment was carried out in a cylindrical plasma source (Supper II—see Fig. 3), which has been described in detail by Brennan, Lehane, *et al.* (1963). It

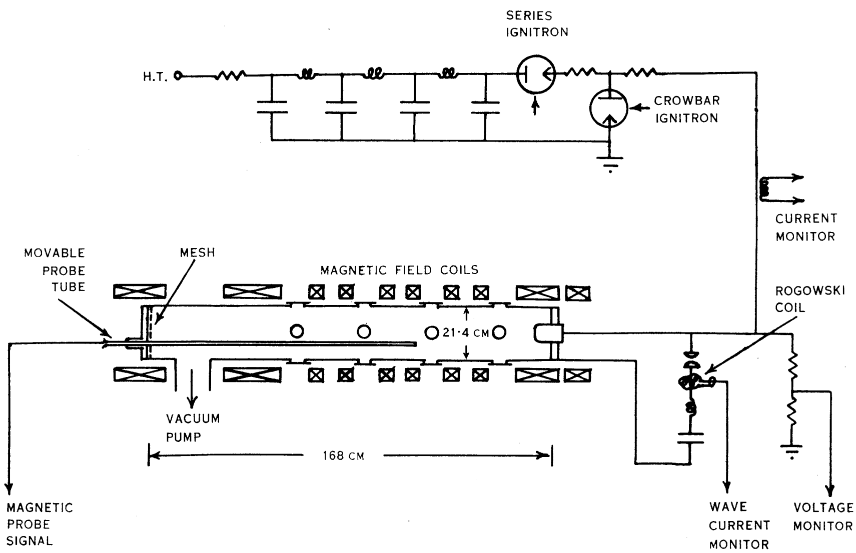

Fig. 3.—Schematic diagram of experimental apparatus (Supper II).

consists of a stainless steel vacuum vessel, through which hydrogen at a pressure of 70 μmHg is circulated. It is immersed in a uniform axial magnetic field of $12 \cdot 8$ kG. One end of the machine is sealed with a quartz plate that has a central molybdenum electrode. The other end is sealed with a Pyrex glass plate to which a stainless steel mesh is attached on the inside. There are 16 radial diagnostic ports along the machine, in 4 groups of 4.

To prepare the plasma, a pulse line of impedance $0 \cdot 7\ \Omega$, charged to $+20$ kV, is discharged through a series resistance of $1 \cdot 05\ \Omega$ to the end electrode; the gas breaks down and a hydromagnetic ionizing shock front, driven by the discharge current of $6 \cdot 3$ kA, travels down the tube. The characteristics of the shock front have been studied here and are reported by Brennan, Brown, *et al.* (1963). Behind the front the plasma is left rotating. This rotation is removed by the "self crowbarring" that occurs when the front hits the stainless steel mesh at the far end (a time of about 50 μs after breakdown). The sudden cessation of rotation of the plasma causes a large-amplitude standing Alfven wave to be set up; this is evidenced by a ringing voltage appearing on the electrode. The plasma preparation current is crowbarred (by an ignitron) on the first positive swing of the electrode, at about 60 μs after breakdown. It has been found from framing camera photographs that a less turbulent plasma is produced if the mesh does the plasma crowbarring, rather than the ignitron; hence the above order of events is used.

(*b*) *Wave Excitation*

The waves are launched at times of 150, 200, or 250 μs after initial breakdown. The wave launcher consists of a condenser of from $0\cdot2\ \mu$F (at 265 kc/s) to $0\cdot01\ \mu$F (at $2\cdot5$ Mc/s), charged to $+20$ kV, in series with a suitable inductance, and discharges via a spark gap to the end electrode and plasma. The ringing circuit is sufficiently isolated from the shorted crowbar ignitron by the inductance of a long coaxial cable. The wave-inducing current is monitored by a Rogowski coil encircling the lead to the spark gap. The peak current for the various condenser–coil combinations is from 1 to 5 kA, and the Q of the circuit varies from about 10 to 20.

(*c*) *Wave Detection*

The wave is detected by a magnetic probe, which is placed inside a quartz tube to isolate it from the plasma. This tube is inserted axially through a hole in the far end plate and mesh at a radius of 5 cm. The probe consists of 30 turns of 40 S.W.G. copper wire on a 2 mm diameter former. It is orientated to pick up the azimuthal component of the wave field, which, theoretically, is the biggest of the three components; this has been confirmed by measuring the other two components.

The wave velocity and attenuation are determined by making measurements of the wave phase and amplitude as a function of axial position. In making these measurements, the probe and the tube are moved together in order to eliminate any possible effect of the tube on the attentuation. Measurements were typically made at five or six different axial positions. For each axial position and time of firing of the waves, between 3 and 12 shots were taken. This was necessitated by the large shot-to-shot variation inherent in the present method of plasma preparation. This scatter increases with frequency and with the axial position of the probe. The stainless steel mesh at the far end did reduce the scatter quite considerably, but still the scatter is as great as (in extreme cases) $\pm50\%$ of the mean value.

(*d*) *Plasma Properties*

To compare the experimental results with the theory outlined in Section II, it is necessary to know the values of the various plasma parameters that occur in the dispersion relation. These parameters are the total particle density, the percentage ionization, the plasma temperature (it is assumed that $T_{\mathrm{e}} = T_{\mathrm{i}}$), and the ion–neutral momentum transfer cross section. Curves of attenuation length *v*. frequency have been drawn from the computed dispersion relation for various sets of these parameters, and the experimental points have been compared with these to find the curve of best fit. The fitting process gives fairly good estimates of the temperature, percentage ionization, and cross section, since the structure of the curves varies in different ways for these three parameters.

Independent estimates of the plasma properties can be obtained. The average ion density across a diameter has been found by measuring the Stark broadening of the Hβ line. A value of about $1 \cdot 6 \times 10^{15}$ cm^{-3} is obtained. This is in reasonable agreement with that expected from the results of Irons and Millar (1965), who have made a detailed investigation of the density and temperature distributions in a similar but smaller machine (Supper I). Their results also enable an estimate to be made of the temperature in Supper II, which has not been measured spectroscopically. This estimated value is $1 \cdot 0$–$1 \cdot 2 \times 10^4$ °K.

These independent estimates of density and temperature are taken only as indications of the correct values. The values obtained from the measured wave velocity and the curve-fitting process described above are thought to be more reliable.

IV. Results

(*a*) *Velocity*

The wave velocity has been measured for three different wave times (150, 200, and 250 μs after breakdown) and for 12 different frequencies. A least squares fit to a straight line has been made for the three wave times and the mean velocity in the low frequency limit has been found. This is 60 ± 3 cm/μs; a small variation of velocity with frequency is expected theoretically, but this is masked by the scatter in the points. The particle density ρ may be obtained from this low frequency velocity using the simple expression for the Alfven speed, $V_{\mathrm{A}} = B_0(\mu\rho)^{-\frac{1}{2}}$, where B_0 is the static magnetic flux density; in the low frequency limit, the exact dispersion relation yields the same density as the simple expression. The density obtained in this manner is $2 \cdot 1 \times 10^{15}$ cm^{-3}. This is the total particle density, since in the low frequency limit the neutral atoms are closely coupled into the wave motion via ion–neutral collisions.

The density of the unionized gas is $4 \cdot 6 \times 10^{15}$ atoms/cm^3, more than twice the measured density of the plasma at the wave time. Spectral measurements made on Supper I can be explained by assuming a large radial drift of particles to the wall during plasma preparation by the $J \times B$ process; this loss of particles is sufficient to account for the difference in densities. The value of $2 \cdot 1 \times 10^{15}$ cm^{-3} for the total particle density has been used in the selection of a curve of best fit for the attenuation results. The shape of the theoretical attenuation–frequency curve is, however, very insensitive to the total particle density.

(*b*) *Attenuation*

The measured attenuation lengths for two wave times, 150 and 250 μs, are shown in Figures 4(*a*) and 4(*b*), together with the finally selected curves of best fit. The plasma parameters appropriate to these curves are:

Total particle density	$2 \cdot 1 \times 10^{15}$ cm^{-3}
Temperature	$1 \cdot 2 \times 10^4$ °K
Radial wave number	$36 \cdot 5$ m^{-1}
Percentage ionization	50%
Collision cross section	$5 \cdot 0$–$10 \cdot 0 \times 10^{-15}$ cm^2

The manner in which the shape of the curve varies with the different parameters ensures the selection of the correct value; the low frequency damping is determined almost entirely by the temperature alone (i.e. by ion–electron collisions), and the fitting of the curve at the low frequency end ensures the correct temperature. The damping of a low frequency Alfven wave is a good diagnostic for temperature; such a technique has been used in this laboratory.

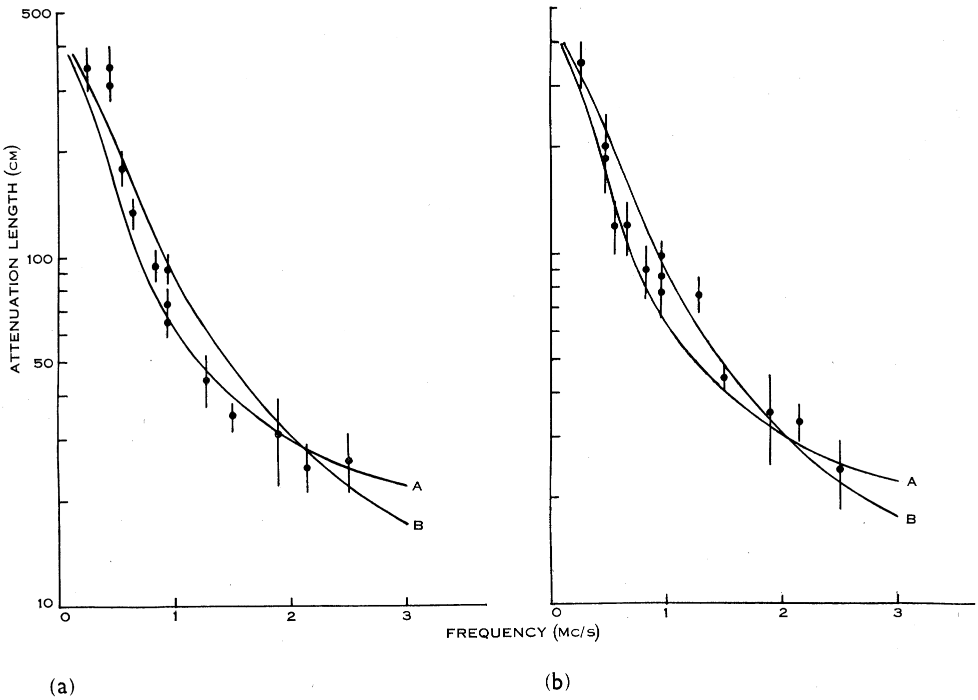

Fig. 4.—Measured attenuation lengths as a function of frequency, for the wave launching times of (*a*) 150 μs and (*b*) 250 μs after plasma preparation. Also shown are the finally selected theoretical curves; these have the following parameters: total particle density $2\cdot1\times10^{15}$ cm^{-3}, fractional ionization $0\cdot5$, temperature $1\cdot2\times10^{4}$ °K, cross sections A $5\cdot0$, B $10\cdot0\times10^{-15}$ cm^{2}.

It is at first surprising that the percentage ionization is about the same for all three wave times; one may have expected this to fall off with time. Irons and Millar (1965) have shown that the plasma decay process occurs much faster in the outer, cooler layers of the plasma, and this leads to a shrinkage in diameter of the central plasma column, within which the density and temperature fall off very slightly during the times of interest. Framing camera photographs show no apparent change in the diameter of the central core. As discussed in Section II(*b*), this results in only a small change in the radial wave number, and the attenuation change is expected to be small.

V. Discussion

It is of interest to compare the momentum transfer cross section obtained here ($7\cdot5\pm2\cdot5\times10^{-15}$ cm^{2}) with other experimental and theoretical estimates. Fite, Smith, and Stebbings (1962) have measured the hydrogen ion–atom charge exchange cross section down to 20 eV ($2\cdot3\times10^5$ °K) by the modulated crossed beams technique. Their points fall more or less uniformly on a straight line that extrapolates back to $5\cdot5\times10^{-15}$ cm^2 at 1 eV ($1\cdot16\times10^4$ °K), with rather large error here. Dalgarno (1960) states that the momentum transfer cross section is equal to twice the charge exchange cross section, and so Fite would predict a momentum transfer cross section of $1\cdot1\times10^{-14}$ cm^2, again with rather large error. Dalgarno arrives at a theoretical value of $1\cdot0\times10^{-14}$ cm^2. Swanson (1963) has conducted a Fourier analysis of the impulse response of a plasma to the compressional hydromagnetic wave. He does not state a cross section, but a calculation based on his results gives the value 5×10^{-15} cm^2 at $\sim$5000°K; the associated error is probably $\pm$2–3×10^{-15} cm^2. The cross section varies slowly with temperature, and the expected difference in values at 5000°K and at 12000°K is only about 10%.

The present experiment, then, yields a momentum transfer cross section that is consistent with both theoretical values and the little experimental data available. The dispersion relation used here, with the deduced value for the cross section, is able to predict the measured attenuation lengths quite well, from frequencies where neutral atoms are unimportant to the wave damping, to frequencies where ion–neutral collisions affect the damping greatly. From equation (11) of the Appendix it can be shown that the momentum vector has a quadrature component, introduced by the neutral particles lagging in phase, varying from less than 1% to nearly 40% of the real component, for the frequency range covered. Thus one can conclude that the roles of ion–electron and ion–neutral collisions have been well identified.

VI. Acknowledgments

The author is grateful to Professor C. N. Watson-Munro and the late B. E. Swire for discussion in the course of this work, to the Institute of Nuclear Science and Engineering for financial support, and to Professor H. Messel for the provision of research facilities in the School of Physics.

VII. References

Alfvén, H. (1942).—*Ark. Mat. Astr. Fys.* **29B**: 1.

Allen, T. K., Baker, W. R., Pyle, R. V., and Wilcox, J. M. (1959).—*Phys. Rev. Lett.* **2**: 383.

Åström, E. (1950*a*).—*Nature* **165**: 1019.

Åström, E. (1950*b*).—*Ark. Fys.* **2**: 443.

Bostik, W. H., and Levine, M. A. (1952).—*Phys. Rev.* **87**: 671.

Brennan, M. H., Brown, I. G., Millar, D. D., and Watson-Munro, C. N. (1963).—*J. Nucl. Energy* C **5**: 229.

Brennan, M. H., Lehane, J. A., Millar, D. D., and Watson-Munro, C. N. (1963).—*Aust. J. Phys.* **16**: 340.

Dalgarno, A. (1960).—*Proc. Phys. Soc.* **75**: 374.

De Silva, A. W. (1961).—Ph.D. Thesis, Univ. Calif. Radiation Lab. Rep. 9601.

Fite, W. L., Smith, A. C. H., and Stebbings, R. F. (1962).—*Proc. Roy. Soc.* A **268**: 527.

Herlofson, N. (1950).—*Nature* **165**: 1020.

Irons, F. E., and Millar, D. D. (1965).—*Aust. J. Phys.* **18**: 23.

Jephcott, D. F., and Stocker, P. M. (1962).—*J. Fluid Mech.* **13**: 587.

Lehnert, B. (1954).—*Phys. Rev.* **94**: 815.

Lundquist, S. (1949).—*Phys. Rev.* **76**: 1805.

Nagao, A., and Sato, T. (1960).—*J. Phys. Soc. Japan* **15**: 735.

Nagao, A., and Sato, T. (1961).—Res. Rept Tohoku University, Sendai, Japan.
Spillman, G. R. (1963).—Ph.D. Thesis, Univ. Calif. Radiation Lab. Rep. 10990.
Spitzer, L. (1962).—"Physics of Fully Ionised Gases." (Interscience: New York.)
Swanson, D. G. (1963).—Calif. Inst. Tech., Tech. Rep. No. 1.
Woods, L. C. (1962).—*J. Fluid Mech.* **13**: 570.

Appendix

Derivation of Dispersion Relation for Hydromagnetic Waves

The plasma model assumed is as stated in Section II. We consider azimuthally symmetric waves in a hydrogenous plasma and neglect all terms of order $(m_e/m_i)^{\frac{1}{2}}$ or less.

The equations of motion for ions, electrons, and neutral particles are obtained from the Boltzmann equation (Spitzer 1962), and are written here as

$$n_i m_i \partial \mathbf{v}_i/\partial t = n_i e\mathbf{E} + n_i e\mathbf{v}_i \times \mathbf{B} + \mathbf{P}^{ie} + \mathbf{P}^{in}, \tag{1}$$

$$n_e m_e \partial \mathbf{v}_e/\partial t = -n_e e\mathbf{E} - n_e e\mathbf{v}_e \times \mathbf{B} + \mathbf{P}^{ei}, \tag{2}$$

$$n_n m_n \partial \mathbf{v}_n/\partial t = \mathbf{P}^{ni}, \tag{3}$$

where subscripts i, e, n refer to ions, electrons, and neutral atoms respectively. n, m, e are the particle densities, particle masses, and the electronic charge; $\mathbf{v}$ is the macroscopic particle velocity vector, $\mathbf{E}$ and $\mathbf{B}$ are the total electric field and magnetic flux density present, and $\mathbf{P}^{ij}$ is the momentum transfer vector—the momentum transferred per unit time and volume from species j to species i. In the derivation of these equations, all non-linear, pressure gradient, and gravitational potential-like terms have been neglected. Electron–neutral collisions have been neglected since $\mathbf{P}^{en} \sim (m_e/m_i)^{\frac{1}{2}}\mathbf{P}^{in}$.

Using the conservation of momentum

$$\mathbf{P}^{ei} = -\mathbf{P}^{ie}, \tag{4}$$

the definition of current density $\mathbf{j}$

$$\mathbf{j} = en(\mathbf{v}_i - \mathbf{v}_e), \tag{5}$$

and the condition of charge neutrality for a hydrogenous plasma

$$n_e = n_i = n, \tag{6}$$

one can obtain from (1) and (2)

$$\rho_i \partial \mathbf{v}_i/\partial t = \mathbf{j} \times \mathbf{B} + \mathbf{P}^{in}, \tag{7}$$

where $\rho_i = n_i m_i$, and terms of order m_e/m_i, ω/ω_{ce} have been neglected (ω_{ce} = electron cyclotron frequency $= eB_0/m_e$). Now define the ion–neutral collision frequency per neutral, ν_{ni}, by

$$\mathbf{P}^{in} = mn_n \nu_{ni}(\mathbf{v}_n - \mathbf{v}_i), \tag{8}$$

where m is taken to be either the neutral or ion mass. The cross section for momentum transfer σ_{ni} is defined in terms of ν_{ni} through the usual expression

$$\nu_{ni} = n_i \sigma_{ni} v_i.$$

Combining (8) and (3)

$$\mathbf{P}^{\mathrm{in}} = \frac{\mathrm{i}\omega\rho_{\mathrm{n}}}{1-\mathrm{i}\tau}\,\mathbf{v}_{\mathrm{i}}, \tag{9}$$

where now $-\mathrm{i}\omega$ replaces the time derivative $\partial/\partial t$, $\rho_{\mathrm{n}} = m_{\mathrm{n}} n_{\mathrm{n}}$, and $\tau = \omega/\nu_{\mathrm{ni}}$. Substituting (9) in (7) gives the required complex equation of motion,

$$-\mathrm{i}\omega\rho_1 \mathbf{v}_{\mathrm{i}} = \mathbf{j}\times\mathbf{B}, \tag{10}$$

where

$$\rho_1 = \rho_0(1+\mathrm{i}\xi), \tag{11}$$

$$\rho_0 = \rho_{\mathrm{i}} + \frac{\rho_{\mathrm{n}}}{1+\tau^2}, \tag{12}$$

and

$$\xi = \frac{\rho_{\mathrm{n}}}{\rho_0}\cdot\frac{\tau}{1+\tau^2}. \tag{13}$$

The physical significance of the equation (10) is evident in that ρ_1 is complex, expressing the fact that the neutrals introduce an out-of-phase component to the momentum vector.

Now using (5) in (1) to eliminate $\mathbf{v}_{\mathrm{e}}$, and again neglecting terms of order $m_{\mathrm{e}}/m_{\mathrm{i}}$, $\omega/\omega_{\mathrm{ce}}$, one obtains the generalized Ohm's law,

$$\mathbf{E}+\mathbf{v}_{\mathrm{i}}\times\mathbf{B} = (1/en)\mathbf{j}\times\mathbf{B}+\boldsymbol{\eta}\cdot\mathbf{j}, \tag{14}$$

where $\boldsymbol{\eta}$ is the resistivity tensor defined by

$$\boldsymbol{\eta}\cdot\mathbf{j} = \mathbf{P}^{\mathrm{ei}}/ne. \tag{15}$$

The resistivity is related to the temperature by the formulae of Spitzer.

The complex equation of motion, equation (10), the generalized Ohm's law, equation (14), and Maxwell's equations,

$$\nabla\times\mathbf{B} = \mu_0\mathbf{j}, \tag{16}$$

$$\nabla\times\mathbf{E} = -\partial\mathbf{B}/\partial t, \tag{17}$$

constitute the set to be solved.

Now let $\mathbf{B} = \mathbf{B}_0+\mathbf{b}$, where $\mathbf{B}_0$ is the static axial field, and $\mathbf{b}$ the perturbation wave field. Putting (10) in (14) and using (16) and (17) to eliminate all wave variables but $\mathbf{b}$, and neglecting all second-order terms, one obtains

$$\mathbf{b}+\frac{V^2}{\omega^2}\nabla\times[\{(\nabla\times\mathbf{b})\times\hat{\mathbf{z}}\}\times\hat{\mathbf{z}}]+\frac{\mathrm{i}}{\omega\mu_0}\nabla\times\{\boldsymbol{\eta}\cdot(\nabla\times\mathbf{b})\}+\frac{\mathrm{i}V^2}{\omega\omega_{\mathrm{ci}}}\cdot\frac{\rho_1}{\rho_{\mathrm{i}}}\nabla\times\{(\nabla\times\mathbf{b})\times\hat{\mathbf{z}}\} = 0, \tag{18}$$

where $V^2 = B_0^2/\mu_0\rho_1$, and $\hat{\mathbf{z}}$ is the unit vector in the axial direction.

Equation (18) can best be solved by making use of a type of vector notation. For any vector $\mathbf{A}$ with a dependence like $\exp \mathrm{i}(pz+m\theta-\omega t)$, with $m = 0$, then in cylindrical coordinates

$$\nabla \times \mathbf{A} = \begin{bmatrix} 0 & -\mathrm{i}p & 0 \\ \mathrm{i}p & 0 & -\dfrac{\partial}{\partial r} \\ 0 & \dfrac{1}{r}\dfrac{\partial}{\partial r}r & 0 \end{bmatrix} \mathbf{A} \tag{19}$$

and

$$\mathbf{A} \times \hat{\mathbf{z}} = \begin{bmatrix} 0 & 1 & 0 \\ -1 & 0 & 0 \\ 0 & 0 & 0 \end{bmatrix} \mathbf{A}. \tag{20}$$

Using these relations, and taking $\boldsymbol{\eta}$ to be of the form

$$\boldsymbol{\eta} = \begin{bmatrix} \eta_\perp & 0 & 0 \\ 0 & \eta_\perp & 0 \\ 0 & 0 & \eta_\parallel \end{bmatrix}, \tag{21}$$

equation (18) can be reduced to a matrix equation in $\mathbf{b}$, containing in the matrix coefficients $\partial/\partial r$ type operators. Now assume a solution of the form

$$\mathbf{b} = (A\mathrm{J}_1(\nu r), B\mathrm{J}_1(\nu r), C\mathrm{J}_0(\nu r)). \tag{22}$$

This is the solution expected from the boundary conditions imposed on $\mathbf{b}$ (that $b_r = 0$ at the wall), and also it is the solution given by the cold, collisionless plasma theory. Equation (22) is substituted in the matrix equation for $\mathbf{b}$, and so three equations are obtained in the three unknowns A, B, and C.

Using $\nabla \,.\, \mathbf{b} = 0$ on equation (22), one obtains

$$\nu A = -\mathrm{i}pC, \tag{23}$$

which can be used to eliminate C. One then has three equations, two of which are identical; this has arisen as a result of dropping the pressure gradient term from the linearized equation of motion, and corresponds to the loss of a further wave type. For sound speeds much less than the Alfven speed (as is the case in the present experiment), this mode is physically irrelevant.

For a non-trivial solution, the two remaining equations in A and B must have zero determinant, and one thus obtains the desired dispersion relation

$$ap^4+bp^2+c = 0, \tag{24}$$

where

$$a = \Omega^2-(1-\mathrm{i}\alpha_\perp)^2,$$

$$b = \nu^2(\Omega^2-1)+\nu^2(\alpha_\perp^2+\alpha_\perp\alpha_\parallel)+2(\omega^2/V^2)(1-\mathrm{i}\alpha_\perp)+\mathrm{i}\nu^2(2\alpha_\perp+\alpha_\parallel),$$

$$c = -\frac{\omega^4}{V^4}+\frac{\omega^2\nu^2}{V^2}+\alpha_\perp\alpha_\parallel\nu^4+\mathrm{i}\alpha_\parallel\left\{\nu^4-\frac{\omega^2\nu^2}{V^2}\left(1+\frac{\alpha_\perp}{\alpha_\parallel}\right)\right\},$$

and $\qquad \Omega = (\rho_1/\rho_i) \,.\, (\omega/\omega_{ci}),$

$$\alpha_\perp = \omega\eta_\perp/\mu_0 V^2, \qquad \alpha_\parallel = \omega\eta_\parallel/\mu_0 V^2.$$

For the simplification $\eta_\perp = \eta_\parallel$, this reduces to the same expression as that used by De Silva (1961) and by Spillman (1963).